



**HAL**  
open science

## The characterisation of an exhumed high-temperature paleo-geothermal system on Terre-de-Haut Island (the Les Saintes archipelago, Guadeloupe) in terms of clay minerals and petrophysics

Gildas Beauchamps, Béatrice Ledésert, Ronan Hébert, Vivien Navelot,  
Alexiane Favier

### ► To cite this version:

Gildas Beauchamps, Béatrice Ledésert, Ronan Hébert, Vivien Navelot, Alexiane Favier. The characterisation of an exhumed high-temperature paleo-geothermal system on Terre-de-Haut Island (the Les Saintes archipelago, Guadeloupe) in terms of clay minerals and petrophysics. *Geothermal Energy*, 2019, 7 (6), 10.1186/s40517-019-0122-y . hal-02200578

**HAL Id: hal-02200578**

**<https://hal.science/hal-02200578>**

Submitted on 30 Aug 2021

**HAL** is a multi-disciplinary open access archive for the deposit and dissemination of scientific research documents, whether they are published or not. The documents may come from teaching and research institutions in France or abroad, or from public or private research centers.

L'archive ouverte pluridisciplinaire **HAL**, est destinée au dépôt et à la diffusion de documents scientifiques de niveau recherche, publiés ou non, émanant des établissements d'enseignement et de recherche français ou étrangers, des laboratoires publics ou privés.



Distributed under a Creative Commons Attribution 4.0 International License

RESEARCH

Open Access



# The characterisation of an exhumed high-temperature paleo-geothermal system on Terre-de-Haut Island (the Les Saintes archipelago, Guadeloupe) in terms of clay minerals and petrophysics

Gildas Beauchamps<sup>1\*</sup> , Béatrice Ledésert<sup>1</sup>, Ronan Hébert<sup>1</sup>, Vivien Navelot<sup>2</sup> and Alexiane Favier<sup>3,4</sup>

\*Correspondence:

gildas.beauchamps@u-cergy.fr

<sup>1</sup> Laboratoire Géosciences

et Environnement Cergy,

Université de Cergy

Pontoise, 1 Rue Descartes,

95000 Neuville-sur-Oise,

France

Full list of author information

is available at the end of the

article

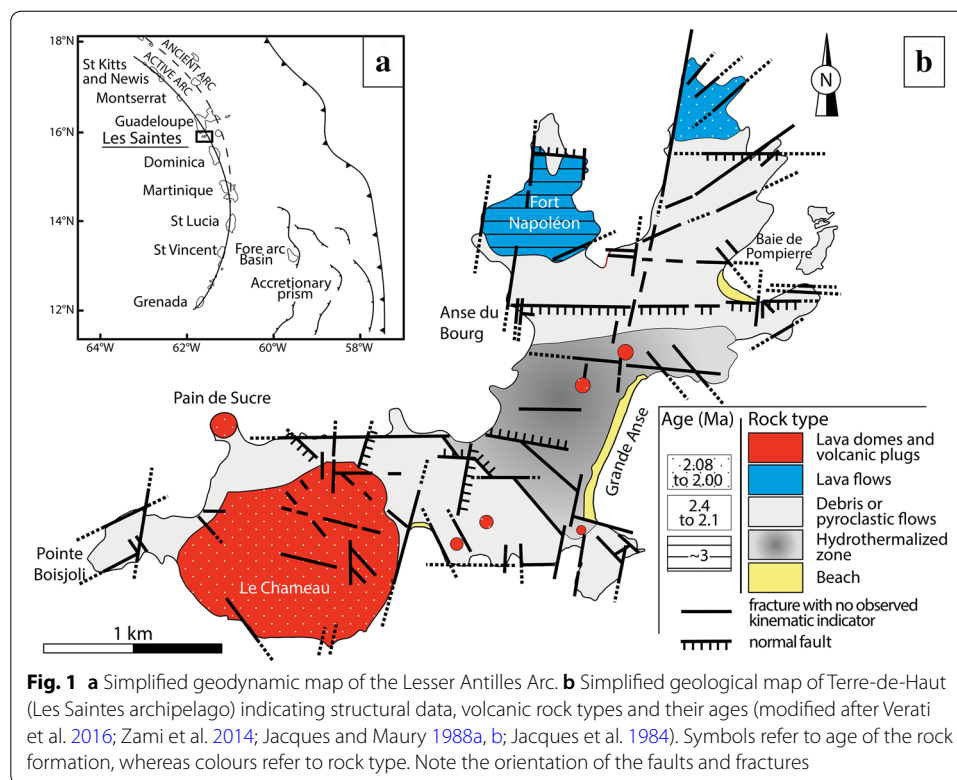
## Abstract

The volcanic island of Terre-de-Haut (in the Les Saintes archipelago, Lesser Antilles arc) is described in the literature as an exhumed paleo-geothermal system. Outcropping conditions provide a good, nearly horizontal 2D view of the system. This present study focuses on clay minerals, as they are known to be good markers of hydrothermal alterations worldwide, and on flow pathways. At Terre-de-Haut, the distribution of the clay minerals has a 'concentric' zonation with smectite, illite and chlorite comprising the outer part to the inner part of the altered zone, respectively. In the active Bouillante geothermal system, located on Basse-Terre island, 35 km NNW of Terre-de-Haut, drillings have revealed a vertical succession of the same clay minerals: from bottom to top, chlorite above 240 °C, illite above 180 °C and smectite at lower temperatures. Both sites have the same clay minerals and can, therefore, be compared. Within those geothermal systems, pathways for the fluids are encountered at all scales, from the micrometre-scale ( $\mu\text{m}$ -scale; through microcracks within phenocrysts and at grain joints) to the metre- and kilometre-scale (m- and km-scale) due to fractures and faults. Petrophysical measurements indicate that fresh rock samples are porous and permeable, allowing hydrothermal alteration on a km-scale. The combination of 1D vertical data at Bouillante and this new 2D horizontal distribution of clay minerals and fractures on Terre-de-Haut allows for a 3D schematic representation of the geothermal systems of the Guadeloupe archipelago and suggests that they are of hectometre-size (hm-size).

**Keywords:** Geothermal systems, Hydrothermal alteration, Clay minerals, Petrophysics, Lesser Antilles, Guadeloupe, Les Saintes

## Introduction

Searching for new geothermal energy resources in the Lesser Antilles and particularly in Guadeloupe (Fig. 1a), it is important to better characterise geothermal systems in this tectonic- and volcanic-active environment. The Bouillante geothermal power plant (Basse-Terre of Guadeloupe) has been producing electricity since 1986 and provides 1D drilling information of the system. Terre-de-Haut (4.5 km<sup>2</sup>, the Les Saintes



archipelago), located 12 km south of Basse-Terre, is described in the literature as exhibiting an exhumed paleo-geothermal system (Jacques and Maury 1988a, b; Verati et al. 2016), giving access to a sub-horizontal 2D cross-section into the system. The combination of the geology of both sites might provide a 3D view of a geothermal system to better understand its fluid pathways. The mineralogy of a hydrothermally altered area on Terre-de-Haut has already been investigated (Jacques and Maury 1988a, b; Verati et al. 2016), but the authors did not focus on clay minerals, which are well known for being good indicators of hydrothermal alterations (Patrier et al. 2003; Mas et al. 2006; Bouchot et al. 2010). This present study focuses on the nature and distribution of clay minerals on Terre-de-Haut to propose a 3D conceptual model of geothermal systems of the Guadeloupe archipelago.

### Geological setting

The Guadeloupe archipelago, located in the Lesser Antilles arc (Fig. 1a), is the result of the subduction of the North American plate under the Caribbean plate at a velocity of approximately  $2 \text{ cm year}^{-1}$  (Hawkesworth and Powell 1980; DeMets et al. 2000; Symithe et al. 2015). Two volcanic arcs result from this subduction (Bouysse 1983): the eastern one corresponds to the outer ancient arc, which was active from the Eocene to Early Miocene; and the western one corresponds to the inner arc, active from the Pliocene. Grande-Terre of Guadeloupe is located on the ancient arc; whereas, Basse-Terre and the Les Saintes archipelago are located on the active arc (Fig. 1a).

Little literature is available about the geology of Terre-de-Haut (Javey et al. 1974; Jacques et al. 1984; Jacques and Maury 1988a, b; Zami et al. 2014; Verati et al. 2016).

Regarding structural data, Verati et al. (2016) recognise four families of fault systems, active from 3 to 2 Ma. They establish a relative chronology, from the oldest to the most recent: (1) N050–N070, (2) N130–N140, (3) N090–N110 and (4) N000–N020 trending fault systems. Kinematic indicators and morphostructural observations demonstrate that the four families of fault systems display normal-slip movements, and three of them have a strike-slip movement (sinistral or dextral) also. The N090–N110 trending fault system is the only one without any evidence for strike-slip movement. Kinematic indicators revealing both dextral and sinistral strike-slips suggest that the N000–N020 and N050–N070 systems were active and reactivated at different stages during the tectonic evolution of the Les Saintes archipelago (Verati et al. 2016). These four families of fault systems affecting the Les Saintes archipelago are compatible with the global tectonic framework of the entire Guadeloupe archipelago (Verati et al. 2016). The 2004 Mw 6.3 Les Saintes earthquake (Beauducel et al. 2005) was correlated with a pure, normal faulting with NW–SE trending nodal planes, which are compatible with the identified onshore N130–N140 faults, indicating that the inherited faults' networks are likely to be reactivated during the present-day plate convergence (Verati et al. 2016).

Regarding the geochronological data, the most recent study (Zami et al. 2014) revealed the presence of three main subaerial volcanic phases on Terre-de-Haut (Fig. 1). The first phase,  $2.98 \pm 0.04$  Ma old, consists of dacitic lava flows and explosive breccia and is located at Fort Napoléon. The second phase, dated at  $2.40 \pm 0.04$  Ma, is widespread across the island, with basic andesitic lava and phreatomagmatic flows associated with two-pyroxene andesite. The third phase, between  $2.08 \pm 0.03$  Ma and  $2.00 \pm 0.03$  Ma, was expressed by the formation of the 'Le Chameau' dacitic dome ( $2.00 \pm 0.03$  Ma) and is associated with some dykes.

The occurrence of a hydrothermal zone has been identified and described (Jacques et al. 1984; Jacques and Maury 1988a, b; Verati et al. 2016). This zone displays a succession of parageneses that are characteristic of high-temperature hydrothermal alteration in epithermal settings and its retrogression during cooling (Verati et al. 2016). Verati et al. (2016) observed a first high-temperature mineral assemblage composed of (i) aggregates of chlorite and epidote developed as pseudomorphs after primary plagioclase and clinopyroxene, or (ii) chlorite, serpentine and oxide aggregates formed at the expense of orthopyroxene. The pseudomorphosed minerals are crosscut by millimetric veinlets filled by quartz  $\pm$  chalcedony  $\pm$  pyrite  $\pm$  chlorite  $\pm$  smectite  $\pm$  goethite aggregates. Sometimes, the veinlets connect vesicles filled with chalcedony and zeolites. A final advanced argillic alteration stage generated kaolinite, illite, smectite, and, in the most altered samples, gypsum and jasper are found (Verati et al. 2016). However, no thorough study of the clay minerals exists to date.

According to Verati et al. (2016), the age of hydrothermalism is constrained within a time span because the oldest volcanic rocks affected by the hydrothermal activity are dated at  $2.40 \pm 0.04$  Ma (Zami et al. 2014), and none of the most recent volcanic plugs dated at  $1.94 \pm 0.10$  Ma by Jacques et al. (1984) is hydrothermally altered, even when located in the hydrothermally altered zone (Fig. 1b, red spots). Hence, Verati et al. (2016) propose that the maximal timescale activity of the Les Saintes paleo-geothermal system is about 400 ky. However, for Zami et al. (2014), the hydrothermal activity lasted around 80 ky between  $2.08 \pm 0.03$  and  $2.00 \pm 0.03$  Ma.

## Materials and methods

The sampling was mainly conducted on outcrops of the second volcanic phase, as hydrothermal activity is restricted to these volcanic rocks (Verati et al. 2016). Additionally three samples from Le Chateau (i.e., late lava dome, Fig. 1) were collected as references. A set of 47 samples was collected in the field (see Fig. 2 and Table 1 for their location), in the apparently most intensely altered zone and its surroundings, either as fracture infillings or in the host rock to better understand how fluids flow through the rocks.

In the following discussion, we call samples in which the volcanic texture is preserved (phenocrysts in a microcrystalline groundmass including plagioclase microlites) as well as the phenocrysts themselves (preservation of main optical property such as morphology, twinning, and birefringence) ‘fresh rocks’ (see Fig. 3a). Fresh rocks are opposed to ‘altered rocks’, which have been submitted to strong hydrothermal alteration, sometimes together with strong fracturing. In altered rocks, the primary volcanic minerals have been completely replaced by newly formed minerals, and the original volcanic texture has been highly or completely overprinted (Fig. 3b).

X-ray Diffraction (XRD) analyses were performed at GeoRessources laboratory (University of Lorraine, France) and at the Institut de Recherche Criminelle de la Gendarmerie Nationale de Cergy-Pontoise (IRCGN, France), both on whole rock and on the  $< 2 \mu\text{m}$  fraction, using a method described by Holtzapffel (1985). The XRD was carried out using a Bruker D2 diffractometer ( $\text{CuK}\alpha$  radiation, 30 kV, 10 mA, GéoRessources) and a Panalytical X’Pert3 Powder ( $\text{CuK}\alpha$  radiation, 45 kV, 40 mA, IRCGN). The analytical conditions used for the acquisition of x-ray diffractograms were as follows: angular domain:  $2\theta =$  between  $2.5^\circ$  and  $30^\circ$  for  $< 2 \mu\text{m}$  fraction, and between  $3^\circ$

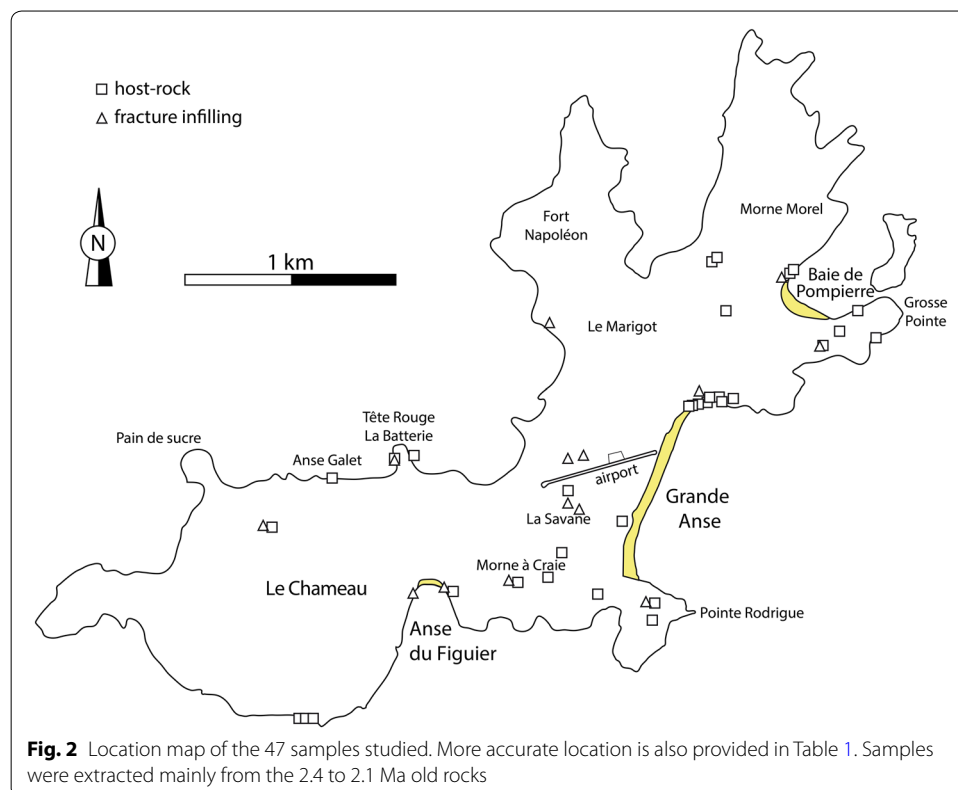
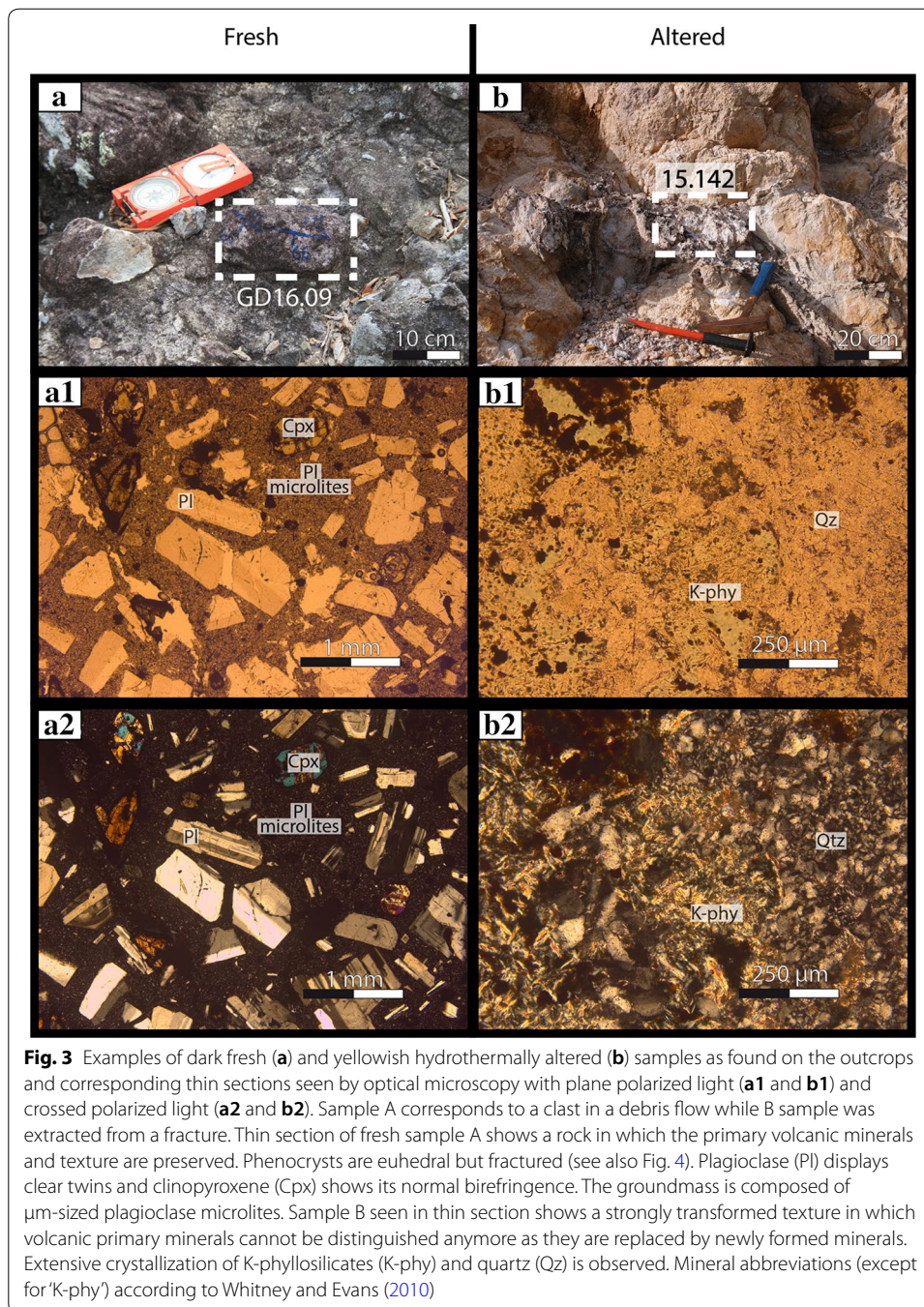


**Table 1 List of samples collected on the field with their occurrence (fracture infillings (F.I.) or host rock (H. R.)), locality, with their GPS coordinates when available, clay mineralogy, and petrophysical parameters [pb: bulk density ( $\text{g cm}^{-3}$ ),  $\Phi_w$ : water porosity (%),  $K$ : permeability ( $\text{m}^2$ , measurement limits  $10^{-19}$ – $10^{-11} \text{ m}^2$ )]**

| Sample   | Occurrence | Locality               | GPS coordinates |               | Clay mineralogy |      |     | Petrophysical properties |                           |              |                        |
|----------|------------|------------------------|-----------------|---------------|-----------------|------|-----|--------------------------|---------------------------|--------------|------------------------|
|          |            |                        | Latitude        | Longitude     | Sme             | Illt | Chl | Kln( $\pm$ Hall)         | ph [ $\text{g cm}^{-3}$ ] | $\Phi_w$ [%] | $K$ [ $\text{m}^2$ ]   |
| 15.142   | F. I.      | Airfied (North)        | N15°51'51.7"    | W061°34'57.8" | ✓               | ✓    | ✓   | ✓                        | 1.90                      | 28.00        |                        |
| 15.144   | F. I.      | Airfied (North)        |                 |               | ✓               |      | ✓   |                          |                           |              |                        |
| GEC 341  | F. I.      | Anse du Figuier (East) | N15°51'30.5"    | W061°35'13.9" | ✓               |      |     |                          |                           |              |                        |
| GEC 342  | H-R        | Anse du Figuier (East) |                 |               | ✓               |      |     |                          |                           |              |                        |
| GD15.136 | F. I.      | Anse du Figuier (West) | N15°51'30.5"    | W061°35'20.8" | ✓               |      |     |                          | 1.60                      | 32.19        |                        |
| GEC 348  | H-R        | Anse Galet             | N15°51'50.1"    | W061°35'36.5" | ✓               |      |     |                          |                           |              |                        |
| 16.10    | H-R        | Grosse Pointe          | N15°52'13.2"    | W061°34'08.6" | ✓               |      |     |                          |                           |              |                        |
| GEC 213  | H-R        | Grosse Pointe          |                 |               | ✓               |      |     |                          |                           |              |                        |
| GEC 217  | F. I.      | Grosse Pointe          | N15°52'13.2"    | W061°34'14.6" | ✓               |      |     |                          |                           |              |                        |
| GEC 219  | H-R        | Grosse Pointe          |                 |               | ✓               |      |     |                          |                           |              |                        |
| 15.147   | H-R        | La Savane              | N15°51'46.9"    | W061°34'55.6" | ✓               |      |     |                          |                           |              |                        |
| GEC 308  | F. I.      | La Savane              |                 |               | ✓               |      |     |                          |                           |              |                        |
| GEC 317  | H-R        | La Savane              |                 |               | ✓               |      |     |                          |                           |              |                        |
| GEC 335  | F. I.      | La Savane              |                 |               | ✓               |      |     |                          |                           |              |                        |
| GEC 337  | F. I.      | North of Le Chameau    | N15°51'43.0"    | W061°35'46.3" | ✓               |      |     |                          |                           |              |                        |
| GEC 338  | H-R        | North of Le Chameau    |                 |               | ✓               |      |     |                          |                           |              |                        |
| GD15.139 | H-R        | Le Chameau (South)     | N15°51'11.7"    | W061°35'39.5" | ✓               |      |     |                          | 2.33                      | 12.94        | $2.94 \times 10^{-14}$ |
| GD15.140 | H-R        | Le Chameau (South)     |                 |               | ✓               |      |     |                          | 2.24                      | 15.64        |                        |
| GD15.141 | H-R        | Le Chameau (South)     |                 |               | ✓               |      |     |                          | 2.45                      | 8.06         | $1.08 \times 10^{-18}$ |
| GEC 220  | H-R        | Le Marigot (East)      | N15°52'14.6"    | W061°34'58.1" | ✓               |      |     |                          |                           |              |                        |
| GEC 221  | F. I.      | Le Marigot (West)      | N15°52'18.4"    | W061°34'24.9" | ✓               |      |     |                          |                           |              |                        |
| GEC 328  | H-R        | Morne a Craie          | N15°51'32.3"    | W061°35'02.3" | ✓               |      |     |                          |                           |              |                        |
| GEC 330  | F. I.      | Morne a Craie          |                 |               | ✓               |      |     |                          |                           |              |                        |

**Table 1 (continued)**

| Sample   | Occurrence | Locality               | GPS coordinates |               | Clay mineralogy |      |     |             | Petrophysical properties |        |                     |                          |
|----------|------------|------------------------|-----------------|---------------|-----------------|------|-----|-------------|--------------------------|--------|---------------------|--------------------------|
|          |            |                        | Latitude        | Longitude     | Sme             | Illt | Chl | Kln(± Hall) | ph [g cm <sup>-3</sup> ] | ØW [%] | K [m <sup>2</sup> ] |                          |
| GEC 331  | H-R        | Morne a Craie          |                 |               | ✓               |      |     | ✓           |                          |        |                     |                          |
| GEC 332  | H-R        | Morne a Craie          |                 |               | ✓               |      |     | ✓           |                          |        |                     |                          |
| GEC 333  | H-R        | Morne a Craie          |                 |               | ✓               |      |     | ✓           |                          |        |                     |                          |
| 16.08    | H-R        | Morne Morel            | N15°52'26.9"    | W061°34'30.7" | ✓               |      |     |             |                          | 2.25   | 17.47               | 1.06 × 10 <sup>-15</sup> |
| 16.09    | H-R        | Morne Morel            |                 |               | ✓               |      |     |             |                          | 2.04   | 22.95               | 1.31 × 10 <sup>-15</sup> |
| GEC 236  | H-R        | Grande Anse (North)    | N15°52'04.1"    | W061°34'31.1" | ✓               |      |     | ✓           |                          |        |                     |                          |
| GD16.01  | H-R        | Grande Anse (North)    |                 |               | ✓               |      |     | ✓           |                          |        |                     |                          |
| GD16.02  | H-R        | Grande Anse (North)    |                 |               | ✓               |      |     | ✓           |                          | 2.07   | 17.11               |                          |
| GD16.03  | H-R        | Grande Anse (North)    |                 |               | ✓               |      |     | ✓           |                          | 2.02   | 26.05               |                          |
| GD16.05  | H-R        | Grande Anse (North)    | N15°52'02.0"    | W061°34'34.8" | ✓               |      |     | ✓           |                          | 2.08   | 22.88               | 1.16 × 10 <sup>-17</sup> |
| GD16.06  | H-R        | Grande Anse (North)    |                 |               | ✓               |      |     | ✓           |                          | 1.97   | 23.55               | 5.26 × 10 <sup>-13</sup> |
| GEC 238  | F. I.      | Grande Anse (North)    |                 |               | ✓               |      |     |             |                          |        |                     |                          |
| GEC 265  | H-R        | Grande Anse (North)    | N15°52'03.9"    | W061°34'32.4" | ✓               |      |     | ✓           |                          |        |                     |                          |
| GEC 270  | H-R        | Grande Anse (North)    |                 |               | ✓               |      |     | ✓           |                          |        |                     |                          |
| GEC 355  | H-R        | Pointe Batterie (East) | N15°51'52.8"    | W061°35'24.0" | ✓               |      |     |             |                          |        |                     |                          |
| GEC 352  | H-R        | Pointe Batterie (West) | N15°51'53.6"    | W061°35'22.1" | ✓               |      |     |             |                          |        |                     |                          |
| GEC 353  | F. I.      | Pointe Batterie (West) |                 |               | ✓               |      |     |             |                          |        |                     |                          |
| GEC 321  | F. I.      | Pointe Rodrigue        | N15°51'29.2"    | W061°34'40.2" | ✓               |      |     |             |                          |        |                     |                          |
| GEC 322  | H-R        | Pointe Rodrigue        |                 |               | ✓               |      |     |             |                          |        |                     |                          |
| GEC 325  | H-R        | Pointe Rodrigue        |                 |               | ✓               |      |     |             |                          |        |                     |                          |
| 17TH27a  | H-R        | Pompierre (NE)         | N15°52'22.9"    | W061°34'18.6" | ✓               |      |     |             |                          |        |                     |                          |
| GD15.137 | F. I.      | Pompierre (NE)         |                 |               | ✓               |      |     |             |                          |        |                     |                          |
| GD15.138 | H-R        | Pompierre (NE)         |                 |               |                 |      |     |             |                          |        |                     |                          |
| GEC 207  | H-R        | Pompierre (SE)         | N15°52'17.8"    | W061°34'07.9" | ✓               |      |     |             |                          | 2.11   |                     | 1.45 × 10 <sup>-15</sup> |



and  $70^\circ$  for whole-rock fraction, step increment:  $2\theta = 0.01^\circ$ , counting time per step: 0.6 s. Each  $< 2 \mu\text{m}$  fraction sample was spread on a glass slide to stack clay minerals on their basal planes. Each sample was analysed in three states: (i) air-dried (natural state); (ii) glycolated for one night to allow swelling of specific clay minerals; and (iii) after heating at  $490^\circ\text{C}$  for 2 h because kaolinite is sensitive to heat (16 selected samples). Furthermore, a formamide test was used to differentiate halloysite from kaolinite (Churchman et al. 1984) on six samples.

Microscopic observations have been done on thin sections using both optical microscopy and scanning electron microscopy (Zeiss Gemini 300).

Petrophysical properties, in particular porosity and density (14 samples) and nitrogen gas permeability (7 samples), were analysed on 25 mm diameter and 21 mm long plugs, under low confining pressure (20 bars). The samples were dried prior to measurements in an oven until a constant weight was reached. The drying temperature was set at 60 °C to avoid any change in mineralogy. Sample preparation is similar to that in Navelot et al. (2018). The measurements were done at Ecole Nationale Supérieure de Géologie (Nancy) (see Table 1). According to Navelot et al. (2018), the permeability measurements did not exhibit Klinkenberg effect (Klinkenberg 1941) and, therefore, no correction was required.

Helium, mercury porosity, and water (triple weight) porosity were measured. Helium porosity was measured using Micromeritics® model AccuPyc II 1340 gas pycnometer. Triple weight porosity measurements were done with distilled water. The porosity data were consistent for each method. In this study, only water porosity data are presented.

Whatever the porosity measurement method employed, the data being consistent ( $\Delta=1.4\%$  in average between water porosity and Helium porosity;  $\Delta=2.6\%$  in average between water porosity and mercury porosity) only triple weight porosity data are presented in the following.

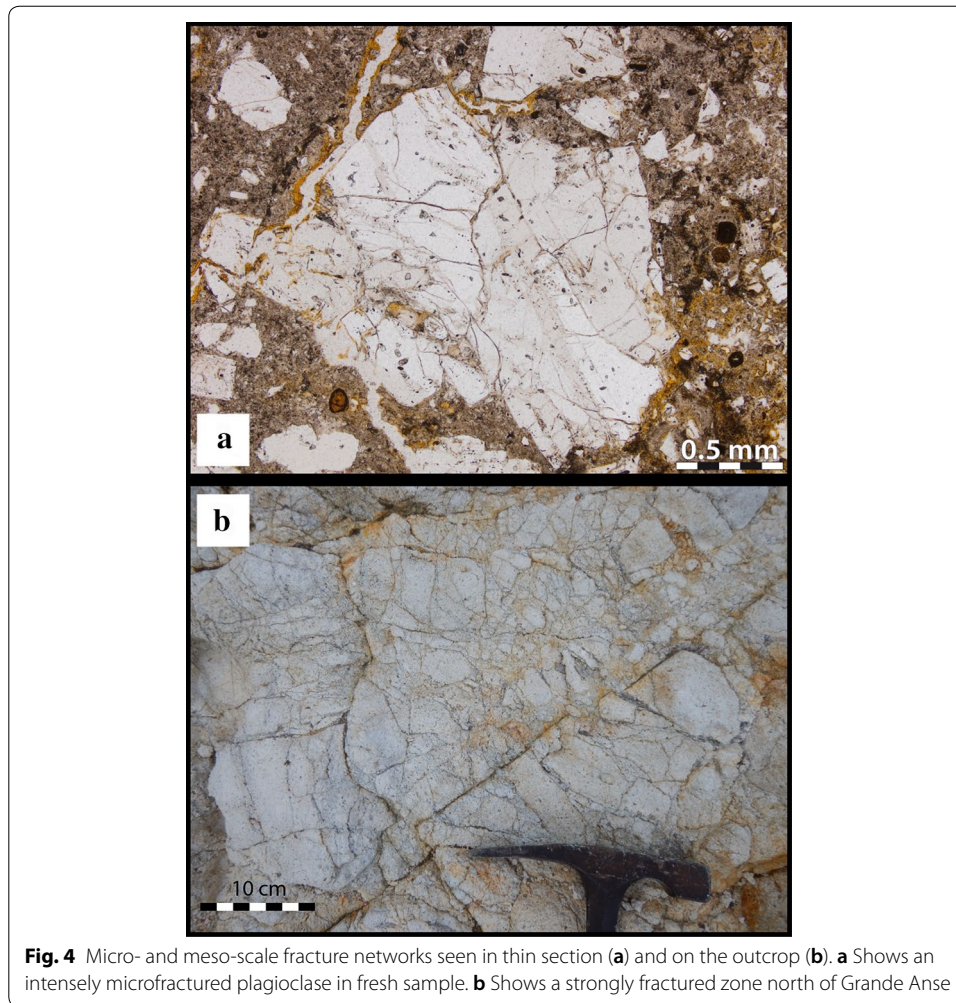
## Results

In the field, rocks have different appearances depending on their alteration state—either fresh or altered. Fresh andesite is darker than the same altered rock, which has a yellowish colour (Fig. 3a, b).

Optical microscopy observations of thin sections from fresh and altered samples display different textures. A ‘fresh’ sample (Fig. 3a) was taken from a clast in a fresh debris flow, while the ‘altered’ sample (Fig. 3b) was taken from a fracture intersecting a completely transformed andesite, where no primary minerals are visible because of strong deformation and alteration.

In the fresh andesitic rock sample (Fig. 3a1 and a2), one can clearly observe a micro-litic groundmass, which represents about 60% of the rock, as estimated by optical observation. Ninety percent of the phenocrysts are made of plagioclase of millimetric size with a euhedral shape frequently displaying a growth zonation. The other phenocrysts are mostly clinopyroxene and orthopyroxene. Opaque minerals are present, as well as amphiboles in some samples. The groundmass is fully microcrystalline and mainly composed of very fine plagioclase crystals. No volcanic glass was observed in our samples, and consistent with previous observations (Navelot 2018; Navelot et al. 2018). Phenocrysts of plagioclase and pyroxenes are strongly microcracked in the fresh sample (Fig. 4a), providing potential pathways for fluid circulation. The porosity of fresh andesite in our samples is related to micropores in the groundmass, as well as microcracks cross-cutting both groundmass and phenocrysts (Fig. 4a), which is in line with Navelot et al. (2018).

In the hydrothermally altered sample (15.142, Fig. 3b, b1, b2), the primary minerals are completely transformed into secondary minerals, such as microcrystalline quartz associated with well-developed K-phyllsilicates (illite or white mica). The Scanning Electron



Microscopy (SEM) observations of this sample (Fig. 5) reveal two types of porosity: microcrack porosity and inter-mineral porosity between K-phylosilicate crystals. In Fig. 5, K-phylosilicate crystals are made of thin crystallites with a fibrous morphology and seem to fill this fracture and bridge it, indicating that they are post-fracturing. In addition, at the outcrop scale, numerous fractures were observed in altered zones, allowing the fluids to flow through the rock (Fig. 4b).

X-ray diffraction analyses performed on whole rock clearly reveal the mineralogical transformation induced by the hydrothermal alteration by comparing the data for a fresh andesite with a hydrothermally altered andesite. The alteration implies the transformation of primary minerals such as plagioclases and pyroxenes, their replacement by clay minerals, and an increase in the relative abundance of quartz (Fig. 6).

Regarding the  $<2 \mu\text{m}$  fraction, the 43 diffractograms acquired can be classified into three main clay assemblages (Fig. 7). Figure 7a contains only smectite (14 Å at natural state, 17 Å when glycolated and 10 Å after heating). Figure 7b contains illite (peak at 10 Å whatever the state of the sample) together with smectite and kaolinite (7 Å peak at natural and glycolated states, no peak when heated). Figure 7c illustrates the presence of chlorite (14 Å peak whatever the state of the sample), illite and smectite.

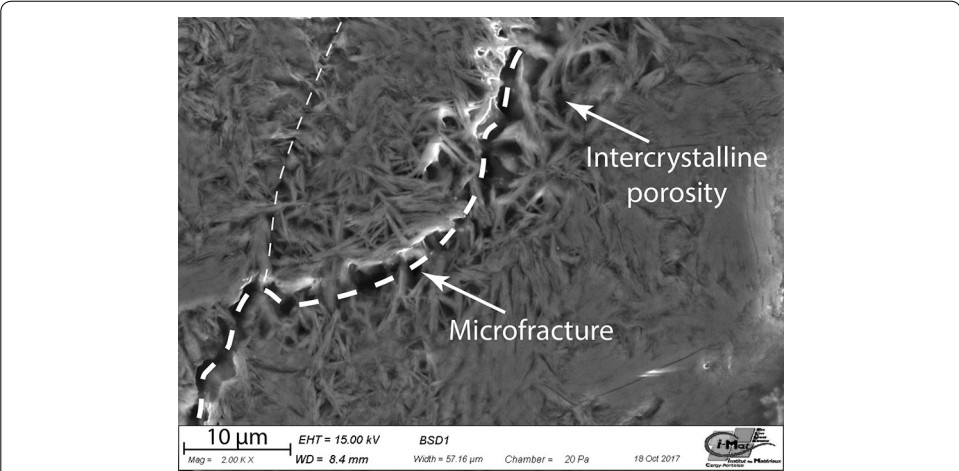


**Fig. 5** Scanning Electron Microscopy (SEM) image of a small zone of altered sample 15.142 showing a total replacement of primary volcanic minerals and groundmass by K-phyllsilicates. Crystallization of K-phyllsilicates is posterior to the development of microfractures as they partially bond them. Intercrystalline porosity is also encountered between K-phyllsilicate crystallites

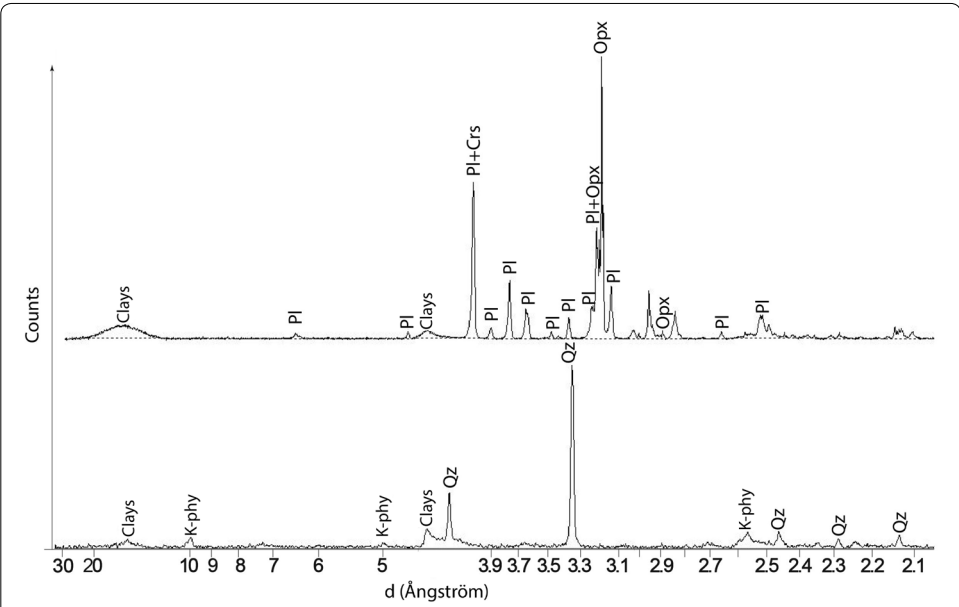
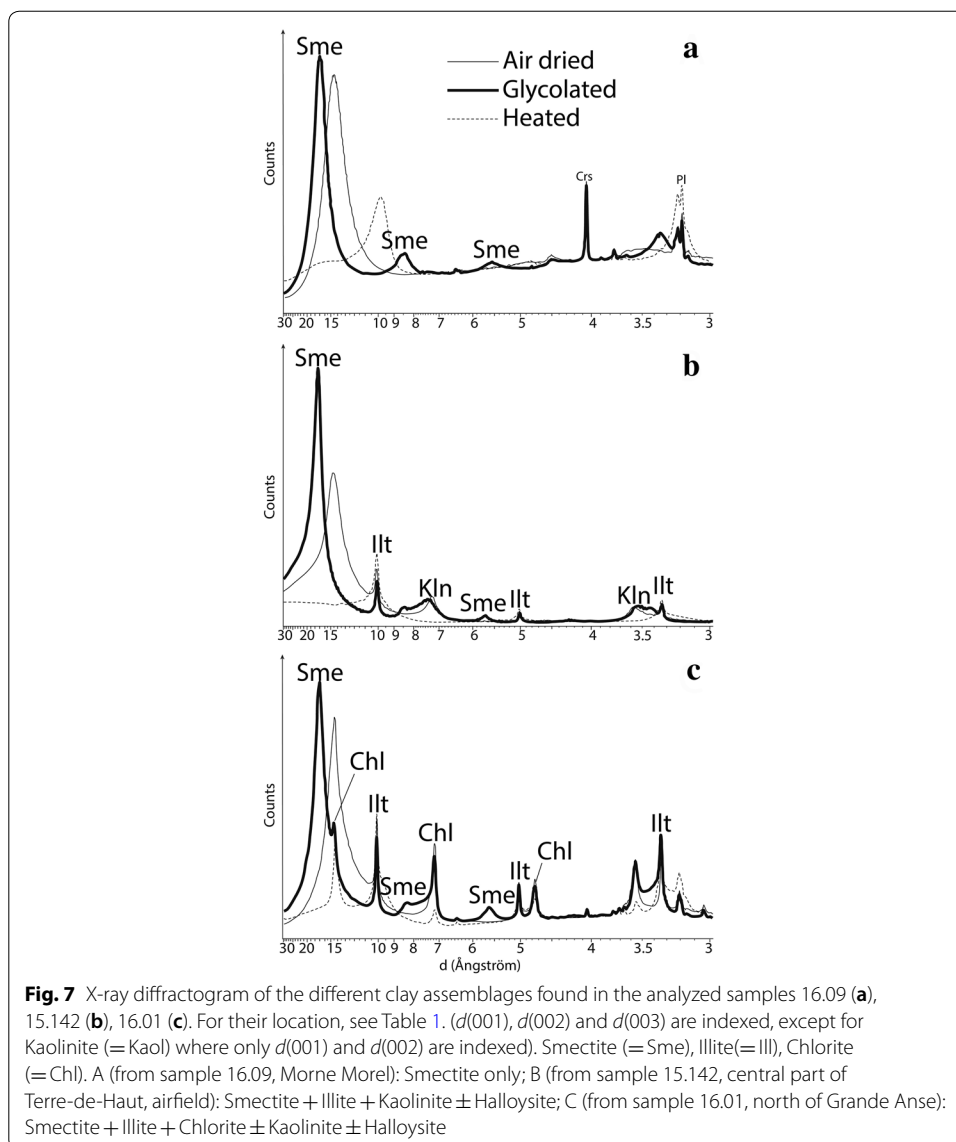


**Fig. 6** X-ray diffractograms performed on whole rock. Comparison of fresh (above) and altered facies (below). *Pl* plagioclase, *Opx* orthopyroxene, *Qz* quartz, *CrS* cristobalite, *K-phy* K-phyllsilicates

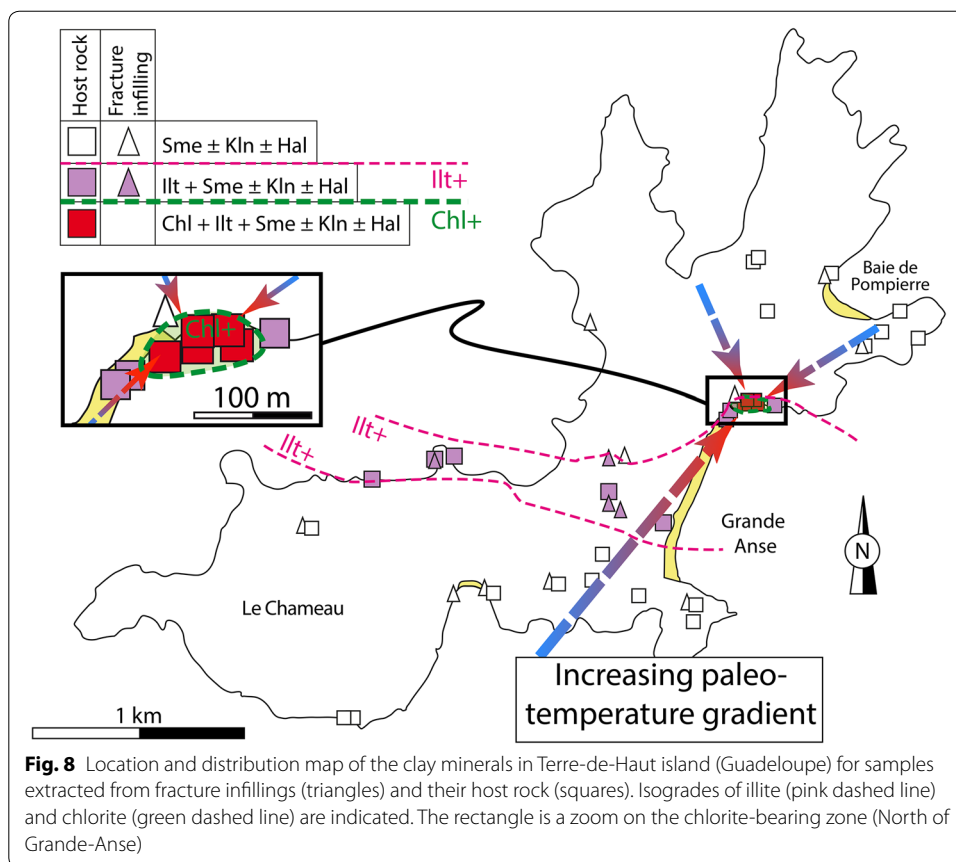
Figure 8 provides the location of each sample with its clay mineral assemblage, and the names of the minerals are provided in decreasing order of abundance. The most widespread assemblage on the island (Fig. 8), which occurs in host rock and in fracture infillings, consists of smectite ± kaolinite ± halloysite (Fig. 7a). This assemblage is called the ‘smectite zone’ in the following discussion. The second assemblage consists of smectite + illite ± kaolinite ± halloysite (Fig. 7b), and is called the ‘illite zone’. This second zone’s extension is more restricted; it crops out along a band that is hundreds of metres wide, orientated east–west, and cuts across the centre of the island (Fig. 8).



The third assemblage, which consists of smectite + chlorite + illite  $\pm$  kaolinite  $\pm$  halloysite (Fig. 7c), is only observed on the east side of the island, north of Grande Anse (Fig. 8), and is called the ‘chlorite zone’. According to this study, this assemblage has the narrowest geographical distribution. The distribution of clay minerals allows us to distinguish the three different zones (Fig. 8).

No difference is apparent in the mineralogy between samples from fracture infillings and the surrounding rocks.

The effective porosity measured on 14 samples from Terre-de-Haut ranges from 6% for the fresh andesite, up to 36% for the most altered sample. The porosity values range is as follows: (i) for smectite bearing samples, 8% to 32%; (ii) for smectite + illite bearing samples, 23% to 28%; (iii) for smectite + chlorite + illite bearing samples, 17% to 26%. Reference samples collected at Le Chateau have 8% to 15% porosity.



Dry bulk density values range from 2.45 g cm<sup>-3</sup> for the fresh sample, to 1.60 g cm<sup>-3</sup> for the most altered sample. The highest densities measured belong to andesite that did not experience strong weathering or hydrothermal alteration. Regarding the samples located in the hydrothermal zone, three are composed of smectite + illite, and their density is between 1.90 and 2.08 g cm<sup>-3</sup>; two have a mineralogical assemblage of smectite + illite + chlorite and are 2.02 g cm<sup>-3</sup> and 2.07 g cm<sup>-3</sup> of density. The lowest density (1.60 g cm<sup>-3</sup>) was measured in a sample located in Anse Figuier, which is outside the central hydrothermally altered zone, where the rock could have experienced a low-temperature alteration.

Nitrogen gas permeability measurements performed on seven samples, either fresh or altered, reveal six orders of magnitude, from 10<sup>-18</sup> to 10<sup>-13</sup> m<sup>2</sup>, between the least and the most permeable samples (Table 1). The sample with the lowest permeability (10<sup>-18</sup> m<sup>2</sup>) (collected at Le Chameau) shows the lowest porosity (8%). However, for the other samples, no relationship between connected porosity and permeability appears. For example, for the three samples with a porosity around 23%, their permeability ranges on four order of magnitudes, from 10<sup>-13</sup> to 10<sup>-17</sup> m<sup>2</sup>.

### Discussion

According to optical microscopy observations and whole-rock XRD analyses, hydrothermal alteration associated with an intense deformation implies a complete transformation of the texture of the rock. Fluids transformed the primary minerals, but may no longer be present in the case of intense hydrothermal circulation. The same process has

also been observed in samples from Bouillante drillings (Mas et al. 2006). In Terre-de-Haut, this whole-rock transformation is generally associated with strong fracturing and the formation of clay minerals.

By comparison with the data from Bouillante geothermal field, and according to Bouchot et al. (2010), the presence of chlorite corresponds to a temperature of crystallization above 240 °C, illite to temperatures higher than 180°, and smectite to temperatures lower than 180 °C.

The distribution of the clay assemblages and the estimated temperatures for each zone suggests a lateral paleo-temperature gradient increasing from the smectite zone to the chlorite zone through the illite zone. Thus, isogrades of mineral appearance can be proposed for illite and chlorite (Fig. 8).

As stated in Patrier et al. (2003) and Opfergelt et al. (2012), kaolinite and halloysite result from meteoric weathering in Basse-Terre, and, therefore, they are not considered in this study.

According to Verati et al. (2016), the hydrothermally altered zone is controlled by the intersection of two normal fault families orientated N090–N110 and N130–N140, north of Grande Anse. These two faults are responsible for the collapse of this zone and are associated with hydrothermal fluid circulation. By comparison of Fig. 1 with Fig. 8, we can now add that this specific area corresponds to the highest temperature recorded and is preserved by clay minerals within the paleo-hydrothermal system.

In Fig. 9, the petrophysical properties of our rocks are compared with data from geothermal fields in similar geological contexts.

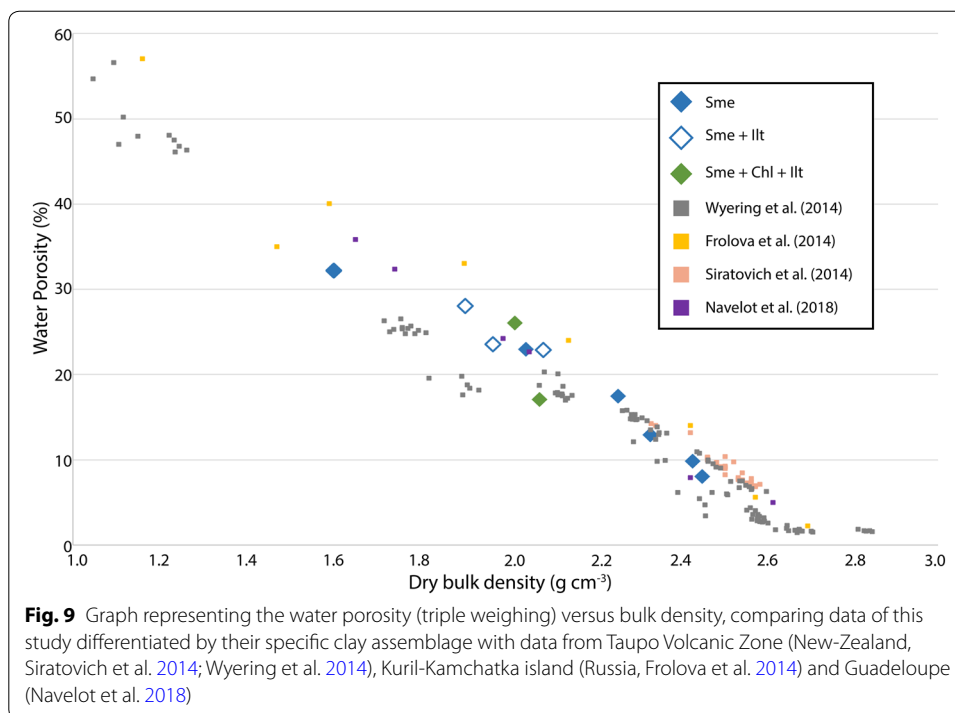
Figure 9 displays the relationship between porosity and bulk density from Terre-de-Haut, the Taupo volcanic zone (New-Zealand, Wyering et al. 2014; Siratovich et al. 2014), Kuril-Kamchatka island (Russia, Frolova et al. 2014) and Guadeloupe (Navelot et al. 2018).

In the Taupo volcanic zone (Wyering et al. 2014), Kuril-Kamchatka island (Frolova et al. 2010, 2014) and in the Darajat geothermal field (West Java, Indonesia, Rejeki et al. 2005), the alteration mineral assemblage and clay type play an important role in enhancing or reducing the primary porosity and density of the rocks.

Low to moderate temperature alteration increases the porosity and decreases the density of the rock; whereas, a high-temperature alteration hardens the rock, leading to a decrease in porosity and an increase in density (Frolova et al. 2010, 2014).

Data from Terre-de-Haut are distributed along the general trend describing a porosity-density linear relationship similar to the one observed in the other locations: the higher the density, the lower the porosity, and vice versa.

The more porous and less dense rock contains only smectite, confirming observations of Wyering et al. (2014). However, samples collected at Le Chameau, also containing smectite, have high density and low porosity. The Le Chameau formation, being more recent than hydrothermal alteration (Zami et al. 2014), means that we can conclude that smectite originates from weathering. In contrast to Wyering et al. (2014), who suggest that chlorite-silica alteration decreases porosity and increases density compared with illite alteration, our illite- and chlorite-bearing samples display similar values of porosity and density and cannot be distinguished. In the Rotokawa geothermal field (New-Zealand), the behaviour of petrophysical properties is mainly



determined by the presence and intensity of microfracturing and seems to be largely independent of the alteration mineralogy, as Siratovich et al. (2014) observed similar alteration intensities (dominated by chlorite/epidote) in the different samples they analysed. The same behaviour might be observed on Terre-de-Haut.

Regarding the nitrogen gas permeability data, no relationship between clay mineralogy and permeability can be deduced from our measurements. The low permeability of the sample presenting the lowest porosity can be explained by its poorly connected and tortuous network of pores and narrow microcracks (Farquharson et al. 2015; Heap and Kennedy 2016; Kushnir et al. 2016; Heap et al. 2017). On the opposite, the two samples with the highest permeabilities ( $10^{-14} \text{ m}^2$  and  $10^{-13} \text{ m}^2$ ) indeed show the highest porosities (24% and 26%).

However, connected porosity is not correlated with permeability for the other samples, as volcanic rocks present microstructurally complex porosity networks (Farquharson et al. 2015; Heap et al. 2017). This microstructural complexity has not been deeply developed in this study.

From the results presented in this current study, no difference was found in the mineralogy of clays sampled in fracture infillings and in the surrounding rock, indicating that the entire area underwent widespread alteration, both through fractures and in the host rock, which can be explained by the connectivity of the network of multi-scale fractures ( $\mu\text{m}$ - to km-scale). These results do not allow the distinguishing of several hydrothermal events.

Our fracture data (Figs. 4 and 5) suggest that both fresh and hydrothermally altered rocks provide pathways for fluid flow (at  $\mu\text{m}$ -scale to m-scale), which is an important point for geothermal projects (Grant et al. 1982). Unfortunately, our data do not

show striking evidence of correlation between permeability, porosity and degree of alteration.

Combining structural (Verati et al. 2016) and mineralogical data (this study), we propose a schematic representation of geothermal systems in the Guadeloupe archipelago (Fig. 10) based on investigations on land at Terre-de-Haut (outcrops) and drillings from Bouillante (Basse-Terre, Fig. 10a). The Bouillante drillings provide a 1D vertical insight into an active geothermal system (Fig. 10b), revealing a vertical zonation of clay minerals (Mas et al. 2006; Bouchot et al. 2010). This partial view is completed by the 2D planar view of Terre-de-Haut, which has been subjected to erosion and in which a lateral paleo-geothermal gradient was observed (Fig. 10c). Both these sites are consistent with a pluri-hm scale of geothermal systems in the Guadeloupe archipelago (Fig. 10d).

**Conclusion**

The island of Terre-de-Haut exhibits a strongly hydrothermally altered east–west trending zone in the central part of the island. This area is characterised by the occurrence of several clay minerals that allow us to distinguish three different hydrothermal zones organised in a general concentric pattern. From the core to the rim of the area, one can

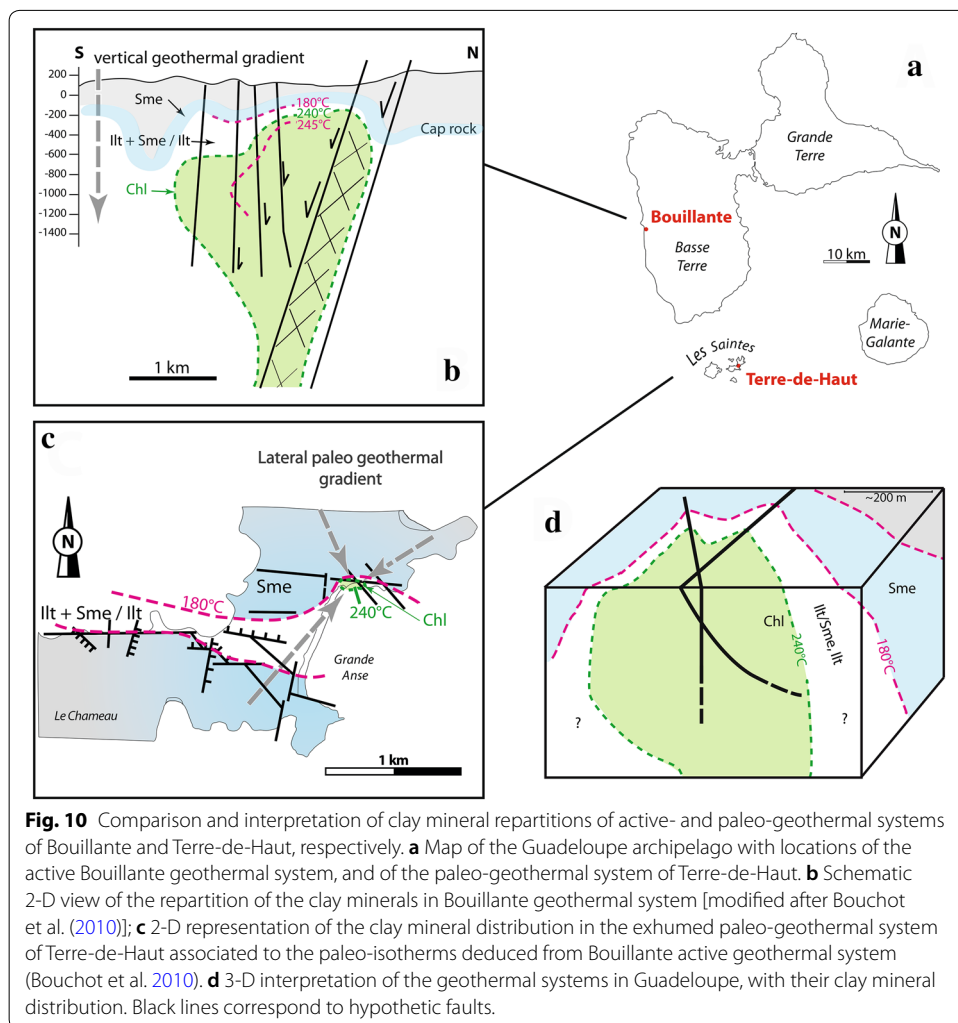


**Fig. 10** Comparison and interpretation of clay mineral repartitions of active- and paleo-geothermal systems of Bouillante and Terre-de-Haut, respectively. **a** Map of the Guadeloupe archipelago with locations of the active Bouillante geothermal system, and of the paleo-geothermal system of Terre-de-Haut. **b** Schematic 2-D view of the repartition of the clay minerals in Bouillante geothermal system [modified after Bouchot et al. (2010)]; **c** 2-D representation of the clay mineral distribution in the exhumed paleo-geothermal system of Terre-de-Haut associated to the paleo-isotherms deduced from Bouillante active geothermal system (Bouchot et al. 2010). **d** 3-D interpretation of the geothermal systems in Guadeloupe, with their clay mineral distribution. Black lines correspond to hypothetical faults.

observe the following: (i) a narrow chlorite zone located north of Grande Anse; (ii) an illite zone elongated in an east–west trend in the central part of Terre-de-Haut (La Batterie, airfield and Savane); and (iii) a large smectite zone that encompasses the two other zones. These clay minerals and their zonation are typical of altered zones in a geothermal context (Stimac et al. 2008; Pola et al. 2012; Frolova et al. 2010, 2014; Wyering et al. 2014). At Bouillante, 35 km NNW of Terre-de-Haut, a similar clay mineral zonation was observed vertically along the boreholes. Since Bouillante is an active geothermal site, the clay mineral zonation observed at Terre-de-Haut can indeed be considered as belonging to an exhumed paleo-geothermal system. The distribution of the clay minerals at Terre-de-Haut describes a paleo-geothermal gradient from the cooler smectite zone to the hotter chlorite zone, with the chlorite zone representing the central part of the reservoir, or at least the hotter preserved hydrothermal alteration zone.

The hydrothermal alteration on Terre-de-Haut appears to be fracture-controlled at all scales, from the km-scale to the  $\mu\text{m}$ -scale. At the km-scale, the extension of the illite zone is controlled to the south (from Anse Galet to La Savane) by N90° and N140° striking faults (Figs. 1 and 10), and to the north of Grand Anse by a N100° striking fault. As at Bouillante, the hydrothermally altered area of Terre-de-Haut is found at the intersection between N90°–N100° and N140° striking faults. At the mesoscale, numerous fractures intersecting each other are observed on the outcrops in the most altered area. At the mm- to the  $\mu\text{m}$ -scale, fresh phenocrysts are strongly microfractured and grain joints in the groundmass also provide pathways for the fluids. In the hydrothermally altered samples, in which primary volcanic minerals have been replaced by newly formed clay minerals, microfractures remain visible, and a porous network appears between the clay crystallites. When one considers the permeability of samples, even fresh samples display relatively intermediate to low values (between  $10^{-14}$  and  $10^{-18}$   $\text{m}^2$ ) because of microfractures and grain joints. The values of altered samples are even higher (up to  $10^{-13}$   $\text{m}^2$ ) because of the porous network between clay mineral crystallites in addition to preserved microfractures. According to Heap and Kennedy (2016), these permeability values likely underestimate the permeability of a volcanic rock-mass, that is crosscut by discontinuities at the outcrop and km-scale such as contacts between volcano-sedimentary units and lava flow, cooling joints, fractures and faults (Navelot et al. 2018).

The combination of Bouillante and Terre-de-Haut petrological data (vertical by drilling and horizontal thanks to outcrops) allows for a 3D representation of geothermal systems in the Guadeloupe archipelago and enables us to estimate their pluri-hectometre size.

Finally, even though the hydrothermally altered zones at Terre-de-Haut and Bouillante are said to be controlled by fractures and their intersections (Calcagno et al. 2012; Verati et al. 2016; this study), no difference has yet been noted in the mineralogy of clays when one compares those found in fracture infillings with those sampled in their host rock. This observation suggests that fluids not only flow through fractures, but also pervasively through rock-effective porosity due to micro- and meso-fractures as well as grain joints. When the rocks are hydrothermally altered, high porosities and permeabilities are measured, indicating that the altered zones might behave as good geothermal reservoirs that can be exploited, such as at Bouillante.

**Authors' contributions**

This study is part of the PhD of GB supervised by BL, RH. VN made petrophysical measurements. VN and AF contributed to field work and interesting discussions. All authors read and approved the final manuscript.

**Author details**

<sup>1</sup> Laboratoire Géosciences et Environnement Cergy, Université de Cergy Pontoise, 1 Rue Descartes, 95000 Neuville-sur-Oise, France. <sup>2</sup> UMR 7359 GeoRessources, Ecole Nationale Supérieure de Géologie, Université de Lorraine, 2 Rue du Doyen Marcel Roubault, Vandoeuvre-lès-Nancy 54500, France. <sup>3</sup> UMR 5243 Géosciences Montpellier, Université des Antilles, Campus de Fouillol, 97159 Pointe-à-Pitre Cedex, Guadeloupe. <sup>4</sup> CNRS, Observatoire de la Côte d'Azur, IRD, UMR 7329 Géoazur, Université Côte d'Azur, 250 rue Albert Einstein, 06560 Valbonne, France.

**Acknowledgements**

Access to XRD both at Université de Nancy and at Institut de la Recherche Criminelle de la Gendarmerie Nationale (IRCGN) is greatly acknowledged. The authors are grateful to unknown reviewers for their helpful comments and suggestions. All the participants of GEOTREF project are thanked for their numerous interactions both in the field and in scientific meetings (GéoAzur, GeoRessources, Teranov, KIDOVA, Mines ParisTech, ENS Paris, IMFT, IPGS, LHyGes, UAG, UCP-GEC).

**Competing interests**

The authors declare that they have no competing interests.

**Funding**

Financial support for this study is provided by the GEOTREF project (<http://www.geotref.com>), and G.B. is grateful for his PhD grant, which is also funded by ADEME in the frame of "Les Investissements d'Avenir" program.

**Publisher's Note**

Springer Nature remains neutral with regard to jurisdictional claims in published maps and institutional affiliations.

Received: 28 August 2018 Accepted: 13 February 2019

Published online: 28 February 2019

**References**

- Beauducel F, Antenor-Habazac C, Bazin S, De Chaballier J-B, Nercessian A, Feuillet N, Jacques E, Bertil D, Boudon G, Lefriant A, Tapponnier P, Hirn A, Lepine J-C, Bernard P, Komorovski J-C, King GCP. The Mw 6.3 earthquake of Les Saintes (Guadeloupe) on November 21, 2004. IAVCEI European Seismological Commission Annual Workshop, Saint-Claude Guadeloupe, 2005; 2005.
- Bouchot V, Traineau H, Guillou-Frottier L, Thinon I, Baltassat JM, Fabriol H, Bourgeois B, Lasne E. Assessment of the Bouillante Geothermal Field (Guadeloupe, French West Indies): Toward a Conceptual Model of the High Temperature Geothermal System. *World Geotherm. Congr.* 2010, Bali, Indonesia; 2010. p. 8.
- Bouysse P (1983) The Lesser Antilles Island Arc: Structure and Geodynamic Evolution. (Service Géologique National), Bureau de Recherches Géologiques et Minières.
- Calcagno P, Bouchot V, Thinon I, Bourguin B. A new 3D fault model of the Bouillante geothermal province combining onshore and offshore structural knowledge (French West Indies). *Tectonophysics.* 2012;526–529:185–95.
- Churchman GJ, Whitton JS, Claridge GGC, Theng BKG. Intercalation method using formamide for differentiating halloysite from kaolinite. *Clays Clay Miner.* 1984;32:241–8.
- DeMets C, Jansma PE, Mattioli GS, Dixon TH, Farina F, Bilham R, Calais E, Mann P. GPS geodetic constraints on Caribbean-North America Plate Motion. *Geophys Res Lett.* 2000;27:437–40.
- Farquharson J, Heap MJ, Varley NR, Baud P, Reuschlé T. Permeability and porosity relationships of edifice-forming andesites: a combined field and laboratory study. *J Volcanol Geotherm Res.* 2015;297:52–68.
- Frolova JV, Ladygin VM, Rychagov SN. Petrophysical alteration of volcanic rocks in hydrothermal systems of the Kuril-Kamchatka Island Arc. In: *Proceedings, World Geothermal Congress 2010, Bali, Indonesia; 2010.* p. 25–29.
- Frolova J, Ladygin V, Rychagov S, Zukhubaya D. Effects of hydrothermal alterations on physical and mechanical properties of rocks in the Kuril-Kamchatka island arc. *Eng Geol.* 2014;183:80–95.
- Grant A, Donaldson IG, Bixley PF. *Geothermal reservoir engineering.* London: Academic Press; 1982.
- Hawkesworth CJ, Powell M. Magma genesis in the lesser Antilles island arc. *Earth Planet Sci Lett.* 1980;51:297–308.
- Heap MJ, Kennedy BM. Exploring the scale-dependent permeability of fractured andesite. *Earth Planet Sci Lett.* 2016;447:139–50.
- Heap MJ, Kennedy BM, Farquharson JI, Ashworth J, Mayer K, Letham-Brake M, Reuschlé T, Gilg HA, Scheu B, Lavallée Y, Siratovich P, Cole J, Jolly AD, Baud P, Dingwell DB. A multidisciplinary approach to quantify the permeability of the Whakaari/White Island volcanic hydrothermal system (Taupo Volcanic Zone, New Zealand). *J Volcanol Geotherm Res.* 2017;332:88–108.
- Holtzapffel T. *Les Minéraux Argileux: Préparation, Analyse Diffractométrique et Détermination*, vol. 12. Lille: Soc. Géol. Nord Publ.; 1985. p. 136.
- Jacques D, Maury R. L'archipel des Saintes (Guadeloupe, Petites Antilles): géologie et pétrologie. *Géologie la Fr.* 1988a;2–3:88–99.
- Jacques D, Maury R. Carte géologique au 1/20 000e, département de la Guadeloupe, Les Saintes. BRGM, Service Géologique National: Orléans; 1988b.
- Jacques D, Maury RC, Bellon H. Géologie et géochronologie des îles des Saintes, Guadeloupe. *CR Acad Sci, Paris, serie II.* 1984; 299, 11, 721–6.

- Javey C, Alsac C, collaboration Mervoyer B. Excursion A6, livret-guide des excursions dans les F.W.I. In: Ville Conf. of Géol. des Caraïbes; 1974. p. 65–72.
- Klinkenberg L.J. The permeability of porous media to liquids and gases. New York: Drilling and Production Practice; 1941. p. 200–13.
- Kushnir AR, Martel C, Bourdier JL, Heap MJ, Reuschlé T, Erdmann S, Komorowski JC, Cholik N. Probing permeability and microstructure: unravelling the role of a low-permeability dome on the explosivity of Merapi (Indonesia). *J Volcanol Geotherm Res.* 2016;316:56–71.
- Mas A, Guisseau D, Patrier Mas P, Beaufort D, Genter A, Sanjuan B, Girard JP. Clay minerals related to the hydrothermal activity of the Bouillante geothermal field (Guadeloupe). *J Volcanol Geotherm Res.* 2006;158:380–400.
- Navelot V. Caractérisations structurale et pétrophysique d'un système géothermique en contexte volcanique d'arc de subduction. Exemple de l'archipel de Guadeloupe. Thesis, University of Lorraine; 2018.
- Navelot V, Géraud Y, Favier A, Diraison M, Corsini M, Lardeaux JM, Mercier de Lépinay J, Legendre L, Beauchamps G. Petrophysical properties of volcanic rocks and impacts of hydrothermal alteration in the Guadeloupe Archipelago (West Indies). *J Volcanol Geotherm Res.* 2018;360:1–21.
- Opfergelt S, Georg RB, Delvaux B, Cabidoche YM, Burton KW, Halliday AN. Mechanisms of magnesium isotope fractionation in volcanic soil weathering sequences, Guadeloupe. *Earth Planet Sci Lett.* 2012;341–344:176–85.
- Patrier P, Beaufort D, Mas A, Traineau H. Surficial clay assemblage associated with the hydrothermal activity of Bouillante (Guadeloupe, French West Indies). *J Volcanol Geotherm Res.* 2003;126:143–56.
- Pola A, Crosta G, Fusi N, Barberini V, Norini G. Influence of alteration on physical properties of volcanic rocks. *Tectonophysics.* 2012;566:67–86.
- Rejeki S, Hadi J, Suhayati I. Porosity study for detail reservoir characterization in Darajat Geothermal Field, West Java, Indonesia. In: Proceedings, World Geothermal Congress, Antalya, Turkey; 2005.
- Siratovich PA, Heap MJ, Villeneuve MC, Cole JW, Reuschlé T. Physical property relationships of the Rotokawa Andesite, a significant geothermal reservoir rock in the Taupo Volcanic Zone, New Zealand. *Geotherm Energy.* 2014;2:10.
- Stimac J, Nordquist G, Suminar A, Sirad-Azwar L. An overview of the Awibengkok geothermal system, Indonesia. *Geothermics.* 2008;37:300–31.
- Symithe S, Calais E, de Chaballier JB, Robertson R, Higgins M. Current block motions and strain accumulation on active faults in the Caribbean. *J Geophys Res Solid Earth.* 2015;120:2014.
- Verati C, Mazabraud Y, Lardeaux J-M, Corsini M, Schneider D, Voitus E, Zami F. Tectonic evolution of Les Saintes archipelago (Guadeloupe, French West Indies): relation with the Lesser Antilles arc system. *Bull Soc Géol Fr.* 2016;187:3–10.
- Whitney DL, Evans BW. Abbreviations for names of rock-forming minerals. *Am Miner.* 2010;95:185–7.
- Wyering LD, Villeneuve MC, Wallis IC, Siratovich PA, Kennedy BM, Gravley DM, Cant JL. Mechanical and physical properties of hydrothermally altered rocks, Taupo Volcanic Zone, New Zealand. *J Volcanol Geotherm Res.* 2014;288:76–93.
- Zami F, Quidelleur X, Ricci J, Lebrun JF, Samper A. Initial sub-aerial volcanic activity along the central Lesser Antilles inner arc: new K-Ar ages from Les Saintes volcanoes. *J Volcanol Geotherm Res.* 2014;287:12–21.

Submit your manuscript to a SpringerOpen® journal and benefit from:

- Convenient online submission
- Rigorous peer review
- Open access: articles freely available online
- High visibility within the field
- Retaining the copyright to your article

---

Submit your next manuscript at ► [springeropen.com](https://www.springeropen.com)

---